



## Paleoenvironmental Conditions of The Chia Gara Formation from Rania Section North Eastern Iraq Using Geochemical Constraints

Flyah H. Al-Khatony<sup>1</sup> , Rafee Ibraheem AL-Hamidi<sup>2</sup> , Safwan F. Al-Lhaebi<sup>3</sup> 

<sup>1,2,3</sup>Department of Geology, College of Science, University of Mosul, Mosul, Iraq.

### Article information

**Received:** 28- Mar -2023

**Revised:** 15- May -2023

**Accepted:** 28- May -2023

**Available online:** 30- June- 2023

#### Keywords:

Paleoproductivity

Redox

Paleoclimate

Paleo-water depth

Hydrothermal activity

#### Correspondence:

**Name:** Rafee Ibraheem AL-Hamidi

**Email:** [rafeege@uomosul.edu.iq](mailto:rafeege@uomosul.edu.iq)

### ABSTRACT

The Chia Gara Formation at Rania section is located in the Shawli anticline near the village of Hangerah in the Rania district of Sulaymaniyah northern Iraq. This section consists mainly of limestone and shale containing organic matter. Geochemical data of major and trace elements were used to constrain paleoenvironmental conditions including paleoproductivity, redox conditions, hydrodynamic conditions, paleoclimate, paleo-water depth, hydrographic conditions, and hydrothermal activity. The productivity proxies (Ba/Al and P/Ti ratios) indicate lower productivity. Redox proxies for trace elements [V/(V+Ni), V/Cr, Ni/Co, and Mo] suggest anoxic to dysoxic marine conditions. The Zr/Rb values indicate roughly that the hydrodynamic energy increased from the lower to the upper section. Sr/Cu and Rb/Sr ratios, which are paleoclimate proxies, indicate semiarid to arid climatic conditions. The Co\*Mn proxies refer to open marine environments associated with upwelling as well as subordinate restricted marine environments. Ni-Zn-Co plot suggests hydrothermal activity during deposition. The Rb/Zr ratio indicates shallowing upward during sedimentation.

DOI: [10.33899/earth.2023.139987.1078](https://doi.org/10.33899/earth.2023.139987.1078), ©Authors, 2023, College of Science, University of Mosul.

This is an open-access article under the CC BY 4.0 license (<http://creativecommons.org/licenses/by/4.0/>).

## الظروف البيئية القديمة لتكوين جياكارا من مقطع رانيا شمال شرق العراق باستخدام المحددات الجيوكيميائية

فليح حسن عباس الخاتوني<sup>1</sup> ID، رافع إبراهيم الحميدي<sup>2</sup> ID، صفوان فتحي المهبي<sup>3</sup> ID  
قسم علوم الأرض، كلية العلوم، جامعة الموصل، الموصل، العراق.

معلومات الارشفة	الملخص
تاريخ الاستلام: 28-مارس-2023	<p>شملت الدراسة الحالية تكوين جياكارا في مقطع رانيا الواقع في طية شاولي بالقرب من قرية هانكيرة في ناحية رانية محافظة السليمانية شمالي العراق. يتكون هذا المقطع بشكل أساسي من الحجر الجيري والسجيل الحاوي على المادة العضوية. تم استخدام البيانات الجيوكيميائية للعناصر الرئيسية والاثرية من أجل تحديد الظروف البيئية القديمة بما في ذلك الإنتاجية القديمة وظروف الأكسدة والاختزال والظروف الهيدروديناميكية والمناخ القديم وعمق المياه القديمة والظروف الهيدروغرافية والنشاط الحرماي. تشير مؤشرات الإنتاجية (نسب Ba/Al و P/Ti) إلى الإنتاجية القليلة. اما مؤشرات الأكسدة والاختزال للعناصر الاثرية [V/(V+Ni), V/Cr, Ni/Co, Mo] فتشير إلى ظروف بحرية لا اوكسجينية الى منخفضة الاوكسجين. في حين ان قيم نسب Zr/Rb فتشير تقريبا إلى زيادة الطاقة الهيدروديناميكية من الجزء السفلي إلى الجزء العلوي. اما نسب Sr/Cu و Rb/Sr، والتي هي مؤشرات المناخ القديم، فتشير إلى الظروف المناخية شبه الجافة إلى الجافة. كما تشير قيم Co*Mn إلى البيئات البحرية المفتوحة المترافقة مع الصعود إلى السطح فضلا عن البيئات البحرية المغلقة الأدنى. ويقترح مخطط Ni-Zn-Co وجود لنشاط المائي أثناء الترسيب. اما نسبة Rb/Zr فتشير إلى التضحل نحو الأعلى أثناء الترسيب.</p>
تاريخ المراجعة: 15-مايو-2023	
تاريخ القبول: 28-مايو-2023	
تاريخ النشر الالكتروني: 30-يونيو-2023	
الكلمات المفتاحية: الإنتاجية القديمة الأكسدة والاختزال المناخ القديم العمق القديم للمياه النشاط الحرماي	
المراسلة: الاسم: رافع إبراهيم الحميدي Email: rafeegeo@uomosul.edu.iq	

DOI: 10.33899/earth.2023.139987.1078, ©Authors, 2023, College of Science, University of Mosul.

This is an open-access article under the CC BY 4.0 license (<http://creativecommons.org/licenses/by/4.0/>).

### Introduction

The Late Jurassic-Early Cretaceous period represents the time when the Chia Gara Formation was deposited, specifically during the Tithonian-Berriasian age. The Balambo-Tanjero zone and the high folded zone in northern Iraq are the areas where the Chia Gara Formation was exposed and is equivalent to several local formations including Karimia, Makhul, and Yamama in the Foot Hill Zone, and Ratawi Formation in central Iraq, and Zubair Formation in the Rutba Uplift Zone. However, no equivalent formations have been recorded in the regional areas due to the lack of exposure and outcrops (Jassim and Buday, 2006).

Wetzel was the first who study the Chia Gara Formation in 1950, in the Chia Gara area South of Amadiya, Dohuk, northern Iraq, within the High Folded Zone. The Chia Gara Formation has a thickness of about 232 meters in its type section and is composed of dark limestone and dark shale rocks due to their organic matter content, limestone, and shale, are rich in ammonite and radiolarian fossils, and the color changes to gray or light yellow, gradually upward. The Chia Gara Formation crops out in several areas in northern Iraq, such as Shiranish, Banki, Ora, Amadiya, Chia Gara, Beakhma, Kork, Barsarin, Rania, Surdash, and Sirwan George. In the sub-surface, the formation was penetrated in the wells of the Kirkuk oil field in the K-109 well, the Qara Jogh-1 well, and the Bai Hassan-81 well (Bellen, et al., 1959).

The Formation in Rania sections consists of a sequence of limestone rocks with shale containing organic matter. The Formation is bounded conformably by the Barsarin Formation

(Kimmeridgian-Early Tithonian) at the bottom. At the top, the Formation is also conformably bounded by the Balambo Formation (Valanginian).

The depositional conditions of ancient sedimentary rocks such as shales have been extensively determined using major and trace element geochemical data (Chen et al., 2019; Kettanah et al., 2020). This article presents geochemical analyses of the Ghia Gara Formation in the Rania section of Northeastern Iraq.

### Aim of the Study

The study aims to assess the conditions of paleoenvironmental that were present when the Chia Gara Formation was deposited in the Rania section of Northeastern Iraq through geochemical constraints.

### Geological Setting

The studied section is located in the Shawli anticline near the village of Hangerah in the Rania district of Sulaymaniyah Governorate, at the intersection of latitude coordinates ( $36^{\circ}17'19.3''\text{N}$ ) and longitude coordinates ( $44^{\circ}51'11.1''\text{E}$ ). The formation in this section is (105) meters thick (Fig. 1).

The rock beds from the Jurassic and Cretaceous periods were exposed and uncovered in the peripheral areas of the High Folded and Thrust Zones, due to the tectonic activity that occurred in northern and northeastern Iraq. The Chia Gara Formation was deposited over a long period, at the end of AP7 and the beginning of AP8, specifically, in two periods (the Late Jurassic and Early Cretaceous), during which important geological events took place. The Jurassic period is considered one of the important periods in geological events, which marked the start of the formation of the new Tethys Sea in the northern and eastern regions of the Arabian Plate (Buday,1980).

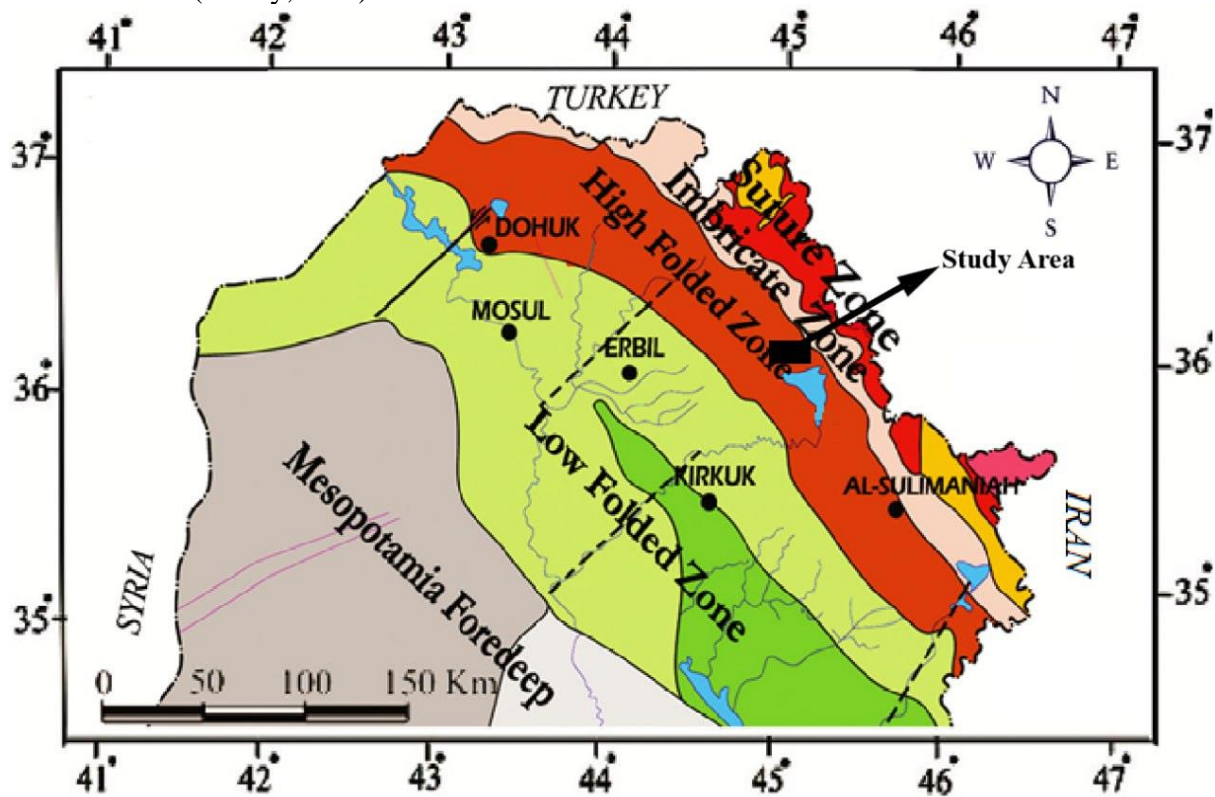


Fig. 1. Tectonic map of the Unstable Shelf zones of Iraq indicating the location of the study area, modified from (Fouad, 2015).

According to (Buday and Jassim, 1987), the Arabian Shelf was divided in the northern part of Iraq into two regions: a stable region, and an unstable region, which was characterized

during the Jurassic period by thrust faulting covered by a thin sedimentary layer that undergoes some discontinuities. These sediments were deposited in toxic, low-oxygen environments. In the Cretaceous period, specifically in the AP8 age, where the Chia Gara Formation was deposited, the Late Tithonian-Berriasian period, when the Sulaiy Formation, which represents the deep internal shelf facies of the Mesopotamian basin, the Mukhul Formation, which represents the outer shelf and deep basin, and the Ghia Gara Formations, which were deposited within the high folds and the Karimia Formation, which is represented by the foothills of the mountains, were the most common (Jassim and Goff, 2006) (Fig.1).

## Materials and Methods

Ten samples of shale from the Rnia section of the Chia Gara Formation are gathered for geochemical analysis. Major and trace elemental analysis was conducted at the German Iraqi laboratory, University of Baghdad/Iraq. Samples were examined using an X-Ray fluorescence spectrometer (Spectro Xepos). Corundum metal was used as the standard material (Ferret et al., 2000).

## Results

### Major Elements

The most abundant major element oxide of the studied samples are SiO<sub>2</sub> (11.47–45.13%, avg. 31.26%), Al<sub>2</sub>O<sub>3</sub> (4.36–21.85%, avg. 11.88%), CaO (14.21–44.54%, avg. 26.9%) and Fe<sub>2</sub>O<sub>3</sub> (1.48–10.81%, avg. 4.11%) while K<sub>2</sub>O, MgO, MnO, Na<sub>2</sub>O, P<sub>2</sub>O<sub>5</sub>, and TiO<sub>2</sub> are less abundant major elements (<2%) (Table 1). The geochemical classification based on (Herron, 1988) was applied to sediments from the Chia Gara Formation using log ratios of SiO<sub>2</sub>/Al<sub>2</sub>O<sub>3</sub> versus Fe<sub>2</sub>O<sub>3</sub>/K<sub>2</sub>O (Fig. 2). This graph shows that the studied samples are chemically categorized as shale and Fe-shale.

**Table 1: The concentrations (wt.%) of major element oxides from the Chia Gara Formation.**

Sample No.	SiO <sub>2</sub>	Al <sub>2</sub> O <sub>3</sub>	CaO	Fe <sub>2</sub> O <sub>3</sub>	K <sub>2</sub> O	MgO	MnO	Na <sub>2</sub> O	P <sub>2</sub> O <sub>5</sub>	TiO <sub>2</sub>
10	11.95	4.36	41.76	3.06	1.67	0.22	0.48	0.54	0.12	0.35
9	38.23	12.96	20.24	2.35	0.55	1.34	0.02	1.07	0.11	0.34
8	31.91	11.42	26.81	4.60	0.50	0.26	0.11	0.31	0.12	0.95
7	33.74	12.07	21.64	4.59	0.76	0.35	0.01	0.40	0.08	1.09
6	34.71	11.91	23.87	1.48	0.42	0.91	0.01	0.72	0.10	0.19
5	39.40	12.31	25.08	2.02	0.45	0.21	0.02	0.21	0.09	0.26
4	11.47	5.37	44.54	2.36	0.36	0.27	0.03	0.52	0.10	0.45
3	39.59	21.85	14.21	10.81	0.79	0.33	0.05	0.25	0.20	1.64
2	45.13	17.68	17.86	5.96	0.62	0.29	0.01	0.18	0.16	1.24
1	26.49	8.87	33.01	3.86	0.85	0.47	0.02	0.46	0.24	0.74
<b>Avg.</b>	31.26	11.88	26.90	4.11	0.69	0.47	0.08	0.46	0.13	0.72
<b>Max</b>	45.13	21.85	44.54	10.81	1.67	1.34	0.48	1.07	0.24	1.64
<b>Min</b>	11.47	4.36	14.21	1.48	0.36	0.21	0.01	0.18	0.08	0.19

### Trace Elements

The concentrations of trace elements in the studied shale samples are listed in (Table 2). The average values of Cr (128.40 ppm), Mo (76.94 ppm), Ba (106.91 ppm), V (495.02 ppm), Ni (112.67 ppm), Cu (52.49 ppm), Zn (130.30 ppm), Rb (23.56 ppm), Sr (576.90 ppm) and Zr (136.62 ppm). These elements are relatively abundant in our samples, whereas other elements such as U, Th, and Co present in low concentration (< 10%) with an average of 3.75 ppm, 8.54 ppm, and 5.79 ppm and ppm respectively.

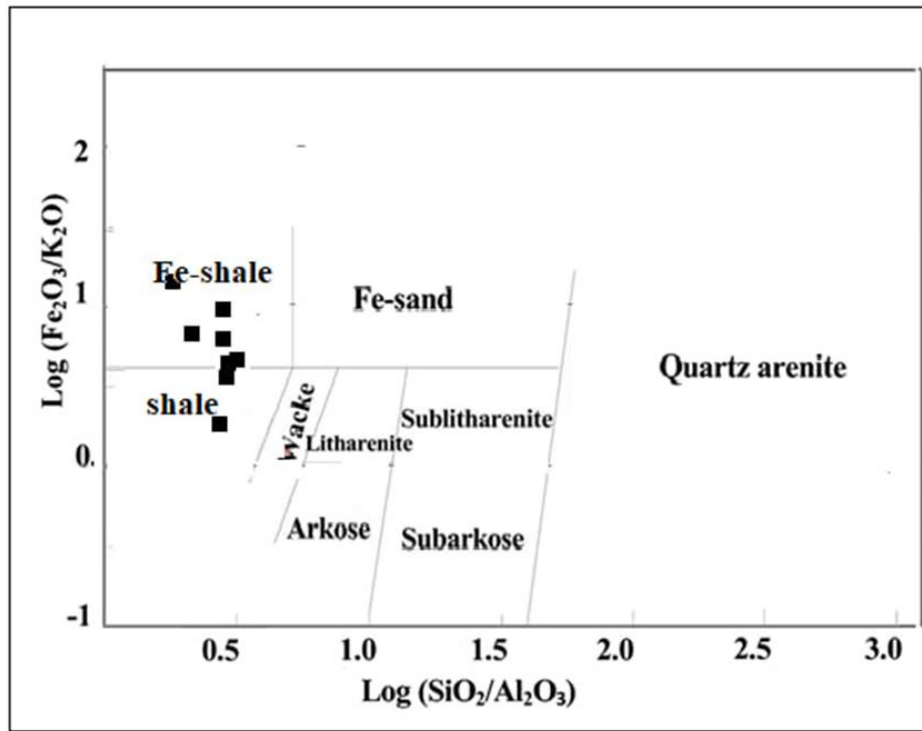


Fig. 2. Geochemical classification of the clastic rocks of the Chia Gara section using the log (SiO<sub>2</sub>/Al<sub>2</sub>O<sub>3</sub>)-log (Fe<sub>2</sub>O<sub>3</sub>/K<sub>2</sub>O) diagram after (Herron, 1988).

Table 2: Trace elements for the Chia Gara Formation, measured in (ppm).

Sample No.	Cr	U	Th	Mo	Ba	V	Co	Ni	Cu	Zn	Rb	Sr	Zr
10	58.02		5.40	36.70	22.00	452.61		74.89	30.60	101.47	9.14	893.79	54.12
9	400.33	5.20	3.20	19.00	201.60	52.66	21.94	47.94	209.70	282.23	19.93	300.36	104.83
8	120.08		12.90	133.00	68.10	1122.0		200.00	49.93	198.52	26.43	798.16	157.54
7	107.69	10.70	12.80	132.40	60.00	902.43	11.40	161.41	39.62	142.68	31.64	593.78	215.13
6	82.72	9.30	2.40	15.80	238.70	23.53	8.97	32.61	15.50	52.78	16.28	261.46	57.45
5	167.29		3.20	12.80	189.70	50.98		41.02	20.05	83.23	17.01	296.13	72.25
4	26.00		4.80	82.20	48.50	285.12		73.63	18.61	46.03	13.35	379.59	55.97
3	154.15	4.40	17.10	28.80	80.60	387.63	8.10	114.73	35.15	146.62	37.95	555.47	301.31
2	98.52	2.60	16.00	110.20	63.00	712.53	7.47	138.70	38.27	114.00	31.18	470.07	227.50
1	69.24	5.30	7.60	198.50	96.90	960.68		241.80	67.42	135.45	32.64	1220.2	120.08
<b>Ave</b>	128.40	3.75	8.54	76.94	106.91	495.02	5.79	112.67	52.49	130.30	23.56	576.90	136.62
<b>Max</b>	400.33	10.7	17.10	198.50	238.70	1122.0	21.94	241.80	209.70	282.23	37.95	1220.2	301.31
<b>Min</b>	26.00	0.00	2.40	12.80	22.00	23.53	0.00	32.61	15.50	46.03	9.14	261.46	54.12

## Discussion

### Paleoproductivity

One of the most important limiting components in the marine environment and a necessary nutrient for plankton is phosphorus (P) (Tyrrell, 1999). P is also an essential component of skeletal tissue and plays a significant role in metabolic processes (Xiao et al., 2020). As a result, it is frequently used to deduce paleoproductivity (Algeo et al., 2011). Another indicator of metabolic activity is Ba, which is also employed to measure marine paleoproductivity (Dymond et al., 1992; Paytan et al., 1996). To reduce the dilution impact of Ba and P from terrigenous clastic materials, the Ba/Al and P/Ti ratios are typically utilized (Shen et al., 2015).

The intake of dissolved inorganic carbon by primary marine producers and its sequestration into organic compounds, as shown by the Ba/Al and P/Ti ratios, is a key indicator of nutritional conditions and paleoproductivity (Tribovillard et al., 2006; Algeo et al., 2011; Li et al., 2020; Zhang et al., 2020). Due to its considerable contribution to skeletal tissue and involvement in a variety of metabolic processes, phosphorus is necessary for all living forms

on earth (Li et al., 2020; Zhang et al., 2021). The availability of organic materials in sedimentary deposits is correlated with P and Ba concentrations, probably due to high productivity (Tribovillard et al., 2006). Paleoproductivity is calculated using Ba/Al and P/Ti ratios since Al and Ti are frequently produced from terrigenous detrital matter (Li et al., 2020). P/Ti values below 0.34 indicate lower productivity, 0.34 to 0.79 indicate intermediate productivity and 0.79 or higher indicates high productivity (Li et al., 2020). In this study, the ratios of Ba/Al and P/Ti vary from 6.73 to 37.86 (avg. 17.80) and 0.05 to 0.39 (avg. 0.18) respectively (Table 3, Fig. 3). Also, Ba/Al and P/Ti curves display similar trend. These values are generally indicating lower productivity.

### **Redox conditions**

Numerous trace elements like U, V, Mo, Ni, and Co demonstrate that the redox state variations in the sedimentary environment also affect their solubility and oxidation state. This has led to their extensive use in reconstructing conditions of the paleoredox for sedimentary rocks and marine sediments (Tribovillard et al., 2006; Algeo and Tribovillard, 2009).

V/ [V+ Ni] ratio is frequently used as a proxy for conditions of redox. When this ratio <0.46 indicates oxic conditions, 0.46 to 0.60 represents dysoxic conditions, between 0.60 and 0.80 refers to anoxic conditions, and > 0.8 implies euxic conditions (Marinez et al., 2015). The shale's V/ [V+ Ni] value ranges between 0.42 and 0.86 (avg. 0.7) (Table 3). These findings indicate that The Chia Gara Formation's shale was deposited in anoxic conditions (Fig. 3).

Additionally, the V/Cr ratio is utilized to evaluate redox conditions, with values greater than 4.25 indicating anoxic (strongly reducing) conditions, from 2.0 to 4.25 indicating dysoxic conditions, and less than 2.0 indicating oxic conditions (Li et al., 2018). The shale's V/Cr ratio in the current study ranges from 0.13 to 13.87 (avg. 6.08) (Table 3), indicating anoxic conditions.

Similarly, Ni/Co values greater than 7.0 indicate a depositional environment is anoxic, between 5.0 and 7.0 a dysoxic environment, and below 5.0 oxic conditions (Guo et al., 2011). Ni/Co value of the shale ranges between 2.19 and 18.57 (avg. 10.54) (Table 3). This value is also denoting anoxic conditions.

The Molybdenum (Mo) concentrations are commonly employed to estimate the redox conditions in both modern and ancient euxic environments (Werne et al., 2002). The value of Mo < 25 ppm reflects oxic conditions (Scott et al., 2017), 25 to 100 ppm indicates intermittent between anoxic and euxic conditions (Helz et al., 2011), >100 ppm suggests permanent euxic conditions (Lyons et al., 2003). The average concentration of Mo in shale for this study is 76.94 ppm with a range of (12.8-198.5 ppm) (Fig. 3; Table 2), this value also supports anoxic conditions.

### **Hydrodynamic Conditions**

The integrating effects of wave base, current velocity, and water depth are known as hydrodynamics, additionally, when hydro energy declines, the amount of organic matter that may be retained in sediments often increases (Hunt 1979). Trace elements such as Zr and Rb are beneficial to infer the conditions of hydrodynamic for the depositional environment. Typically, Zr is depleted in sediments with fine grains but enriched in sediments with coarse grains in the form of zircon (Hu et al., 2017). On the other hand, Rb is primarily deposited in low-energy conditions and accumulates in minerals with fine grains such as clay minerals and mica. Thus, the ratio of Zr/Rb can be used as a proxy indicator to quantitatively reflect hydrodynamic changes. Hence, an environment with high hydro energy is typically indicated by a high Zr/Rb value, and vice versa (Tenger et al., 2006). The values of Zr/Rb in this study are between 3.53 and 7.94 (avg. 5.48) (Table 3; Fig. 3). The curve trend of these value increase from the bottom to the top of the study section, which denotes roughly that the hydro energy increased over time.



## Paleoclimate

Different palaeo-climatic conditions can be distinguished using trace elements sensitive to ancient climatic changes, such as Ba, Co, Cr, Cu, Ni, Sr, Pb, and V (Tao et al., 2017). The ratios of Sr/Cu and Rb/Sr, for example, are trace elemental indicators that are frequently used to infer palaeoclimatic conditions. Generally, Warm, humid climates are often indicated by Sr/Cu ratios between 1 and 5, whereas arid climates are denoted by ratios greater than 5. While Rb/Sr ratios decrease in dry climates, high and low ratios reflect cold and warm climates, respectively (Chen et al., 1999). The ratio of Sr/Cu in this study is greater than 5, and the ratios of Rb/Sr range from 0.01 to 0.07 (avg. 0.05) (Table 3). On the Rb/Sr versus Sr/Cu ratios plot, most of the study samples fall on a semiarid to an arid field (Fig. 4). These facts show that semi-arid to arid climate conditions prevailed when the Chia Gara shale was deposited.

The degree of source rock weathering can also be determined using the Rb/Sr ratios (McLennan et al., 1993). According to (Table 3), the average Rb/Sr ratio in the current study is 0.05, which is less than the averages for UCC (0.33) and PAAS (0.08). This suggests that the source rocks underwent less chemical weathering.

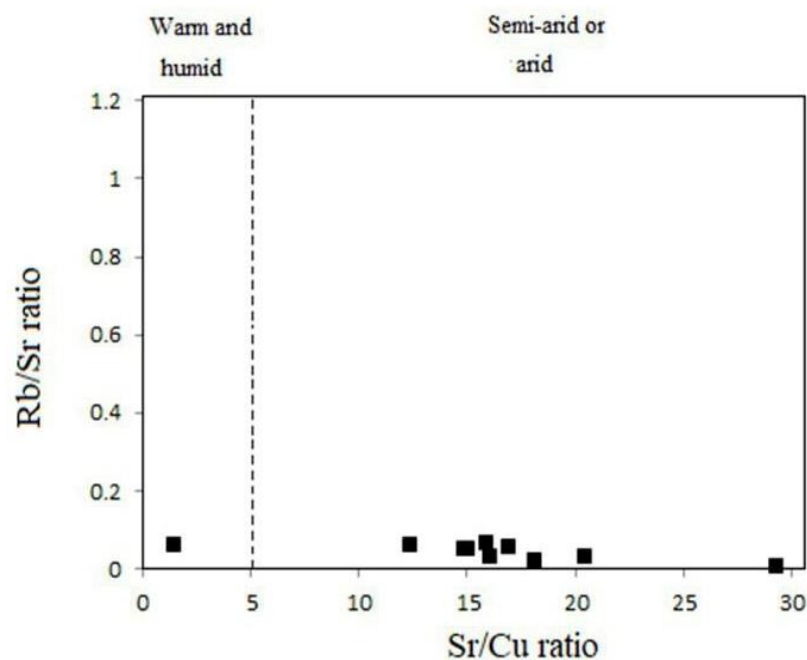


Fig. 4. Paleoclimate discriminating plots comparing Sr/Cu and Rb/Sr after (Li et al., 2021).

Another clue to paleoclimate is the concept of (C-value), which is predicated on the observation that several elements, including Mn, Fe, Ni, Co, Cr, and V are improved in humid environments, while the precipitation of salty minerals causes the concentration of Na, Mg, Ca, K, Ba, and Sr in dry environments (Hu et al., 2017). The formula for determining the C-value is  $C\text{-value} = \frac{[Mn+Fe+Ni+Co+Cr+V]}{[Na+Mg+Ca+K+Ba+Sr]}$  (Ding et al., 2018). When C-value is greater than 0.8, the climate is humid; between 0.6 and 0.8, it is semi-humid; between 0.4 and 0.6, it is semihumid-semiarid; between 0.2 and 0.4, it is semiarid; and below 0.2, it is arid (Zhang et al., 2020). The studied samples exhibited C-values between 0.058 and 0.68 (avg. 0.18) suggesting arid paleoclimate (Table 3). Furthermore, the curve of C-values shows decreasing trend upward which suggests that the climate was becoming more arid than the lower part of the section (Fig. 3).

## Paleo-water depth

The stable element zirconium (Zr), which is present in shale, is commonly transported as detrital zircon. Since its concentration steadily declines from the source region to the sedimentary basin, Zr can be utilized to pinpoint the presence of shale-containing terrigenous

clasts. The content of rubidium (Rb), on the other hand, tends to rise as the water depth increases, and it's an alkaline soil element with a chemical activity that migrates easily and is absorbed by clay minerals (Wang and Guo, 2020). As a consequence, the ratio of Rb/Zr can be utilized to determine the depth of paleo-water. Its higher value, therefore denotes a body of deep water (Loucks and Ruppel 2007). The range of Rb/Zr ratios for the studied samples is 0.13 to 0.28, with an average of 0.20 (Table 3; Fig. 3). It was noted that the largest values are concentrated at the bottom of the section, which indicates that the formation was in a state of relatively upward shallowing during the sedimentation.

### Hydrographic Conditions

Trace elements such as (Mn and Co) have been employed as useful proxies for paleoenvironmental reconstructions to establish the hydrographic state of the sedimentary basin and paleoredoxic conditions (Algeo and Lyons, 2006; Tribovillard et al., 2006). The Co\*Mn proxies were used by (Sweere et al., 2016) to differentiate between hydrographically restricted marginal marine basins and open marine environments associated with upwelling. These authors have demonstrated that Co\*Mn values above 0.4 are typical of hydrographically restricted settings, whereas Co\*Mn values below 0.4 are typical of upwelling settings. In the present study, the Co ppm\*Mn% range from 0.04-1.92 (avg. 0.51) (Table 3). Additionally, the majority of the examined samples, except for one sample, fall in unrestricted upwelling settings, as shown by the plot of Co (ppm)\*Mn (%) versus Al (%) (Fig. 5). These findings suggest that upwelling-associated open marine environments and subordinate restricted marine environments are where the Chia Gara Formation was primarily deposited.

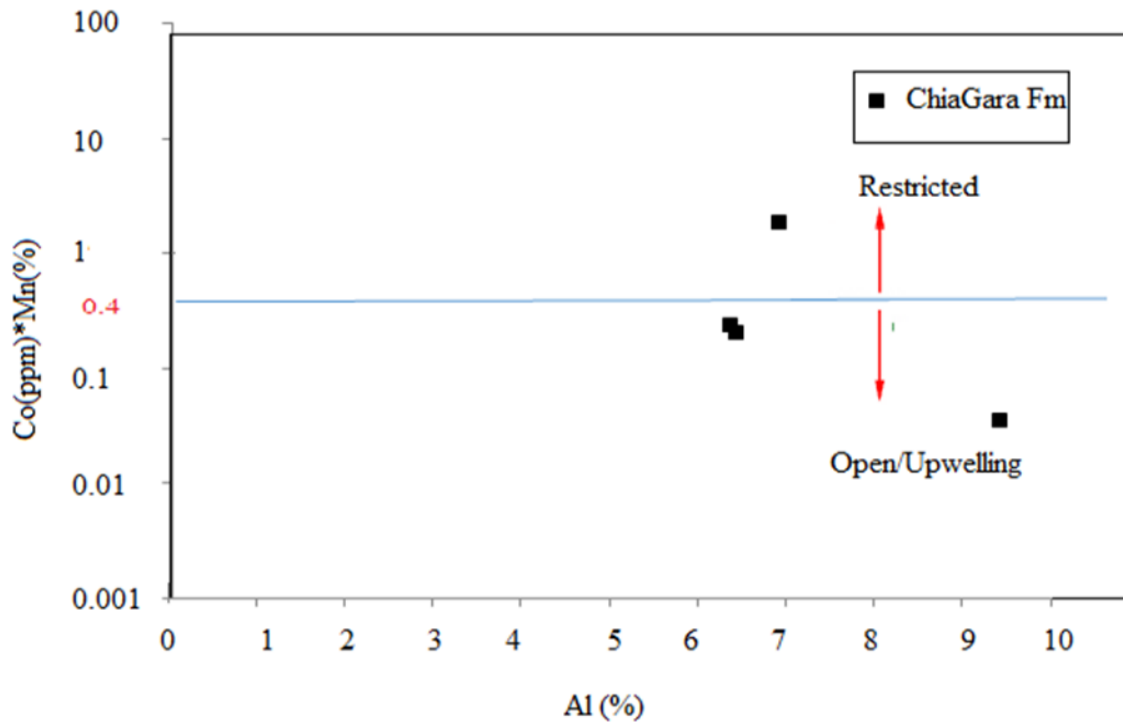


Fig. 5. Diagram of Co (ppm) \* Mn% versus Al% for the studied section after (Sweere et al., 2016).

### Hydrothermal Activity

The typical method for determining if hydrocarbon source rocks have undergone seafloor hydrothermal activity during the early phases of deposition is a Ni-Zn-Co diagram (Choi and Hariya, 1992). This plot is also used to estimate the hydrothermal effect on the sediment during deposition. According to this plot, the hydrothermal field contains most of the studied samples (Fig. 6). This was supported by the tectonic setting of the Northeastern margin of the Arabian plate in the late Tithonian-Cenomanian which was affected by volcanic activity that result from the opening of the Southern Neo-Tethys ocean (Jassim and Goff, 2006). This

could be a breakup unconformity, which is a potential stage for the spreading of the ocean floor during the opening of the Southern Neo-Tethys Ocean. A small microcontinent drifted away as a result of the opening of the Southern Neo-Tethys Ocean, and a new passive margin formed along the northeastern margin of the Arabian Plate.

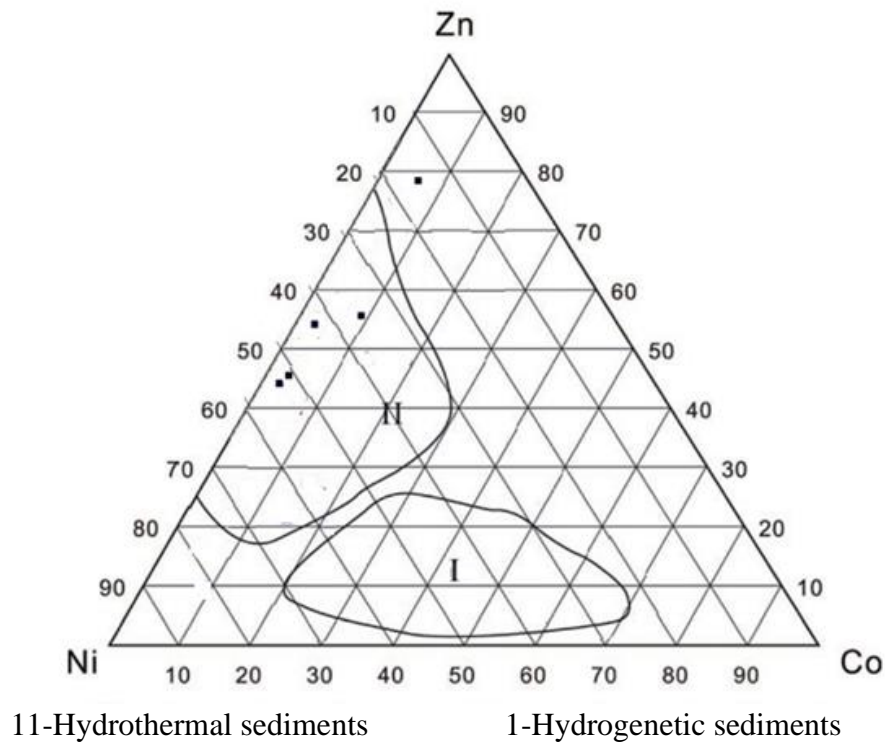


Fig. 6. Ternary diagram showing a comparison of Ni–Zn– Cu Cu constituents of the Chia Gara Formation shales modified after (Chen et al., 2019).

Table 3. Elemental ratios sensitive to environmental conditions for the Chia Gara Formation

Sample No.	Ba/Al	P/Ti	V/[V+Ni]	V/Cr	V/Ni	Ni/Co	Zr/Rb	C- value	Rb/Sr	Sr/Cu	Rb/Zr	Co*Mn
10	9.54	0.24	0.86	7.8	6.04		5.92	0.0805	0.01	29.21	0.17	
9	29.38	0.24	0.52	0.13	1.1	2.19	5.26	0.1077	0.07	1.43	0.19	1.92
8	11.27	0.09	0.85	9.34	5.61		5.96	0.168	0.03	15.99	0.17	
7	9.39	0.05	0.85	8.38	5.59	14.16	6.8	0.2008	0.05	14.99	0.15	0.21
6	37.86	0.39	0.42	0.28	0.72	3.64	3.53	0.058	0.06	16.87	0.28	0.24
5	29.12	0.24	0.55	0.3	1.24		4.25	0.0793	0.06	14.77	0.24	
4	17.05	0.15	0.79	10.97	3.87		4.19	0.0521	0.04	20.39	0.24	
3	6.97	0.09	0.77	2.51	3.38	14.16	7.94	0.6788	0.07	15.8	0.13	0.14
2	6.73	0.09	0.84	7.23	5.14	18.57	7.3	0.3132	0.07	12.28	0.14	0.04
1	20.65	0.23	0.8	13.87	3.97		3.68	0.1133	0.03	18.1	0.27	
<b>Ave</b>	17.80	0.18	0.7	6.08	3.66	10.54	5.48	0.18	0.05	16.18	0.2	0.51
<b>Max</b>	37.86	0.39	0.86	13.87	6.04	18.57	7.94	0.678	0.07	29.21	0.28	1.92
<b>Min</b>	6.73	0.05	0.42	0.13	0.72	2.19	3.53	0.058	0.01	1.43	0.13	0.04

## Conclusion

The Chia Gara Formation in the Rania section of northeastern Iraq is primarily composed of limestone rocks with shale rocks. Geochemical investigations of the shale units were carried out to constrain paleoproductivity, redox conditions, hydrodynamic conditions, paleoclimate, paleo-water depth, hydrographic conditions, and hydrothermal activity. The ratios of Ba/Al and P/Ti are generally denoted by low productivity. Anoxic to dysoxic marine conditions are indicated by redox proxies for trace elements V/ [V + Ni], V/Cr, Ni/Co, and Mo. The Zr/Rb values indicate roughly that the hydro energy increased from the lower to the upper section. The proxies for paleoclimate (C-value, Sr/Cu, and Rb/Sr ratios) suggest semiarid to arid climatic conditions through the deposition of the Chia Gara sediments. The deposition on the

continental margin is primarily in open marine settings related to upwelling and subordinate restricted marine settings, according to the use of the Co\*Mn proxies. Using Ni–Zn–Co ternary diagram suggests the Chia Gara Formation was affected by the hydrothermal solution during deposition. The Rb/Zr indicates that the formation was in a state of relatively upward shallowing during the sedimentation.

### Acknowledgments

We are grateful to the German Iraqi laboratory at the University of Baghdad / Iraq for its assistance in conducting the necessary analyses for the current study, especially Dr. Hassan Ali from the Department of Geology, Baghdad University.

### Conflict of Interest

The authors declare that they have no financial or close personal relationships that may have seemed to influence the research described in this work.

### References

- Algeo, T.J., and Lyons, T.W., 2006. Mo-Total Organic Carbon Covariation in Modern Anoxic Marine Environments: Implications for the Analysis of Paleoredox and Paleohydrographic Conditions. *Paleoceanogr.* 21, PA 1016, <https://doi.org/10.1029/2004PA001112>.
- Algeo, T.J., and Tribovillard, N., 2009. Environmental Analysis of Paleoceanographic Systems Based on Molybdenum-Uranium Covariation. *Chem. Geol.* Vol.268, pp.211–225. <https://doi.org/10.1016/j.chemgeo.2009.09.001>.
- Algeo, T.J., Kuwahara, K., Sano, H., Bates, S., Lyons, T., Elswick, E., Hinnov, L., Ellwood, B., Moser, J., Maynard, J.B., 2011. Spatial Variation in Sediment Fluxes, Redox Conditions, and Productivity in the Permian-Triassic Panthalassic Ocean. *Palaeogeogr, Palaeoclimatol. Palaeoecol.* Vol. 308, pp. 65–83. <https://doi.org/10.1016/j.palaeo.2010.07.007>.
- Bellen, R.C. van, Dunnington, H.V., Wetzel, W., Morton, D.M., 1959. *Lexique Stratigraphique International, Asie, Fasc. 10a, Iraq.* Centre Natl. Rech. Scii., Paris, 333 P.
- Buday T., and Jassim S. Z., 1987. *The Regional Geology of Iraq. Tectonism, Magmatism, and Metamorphism.* Geological Soc Iraq.
- Buday, T., 1980. *The Regional of Iraq. Stratigraphy and Palaeogeography.* Dar Al-Kutub Publishing House, University of Mosul, Mosul, Iraq 445 P.
- Chen, J., An, Z., Head, J., 1999. Variation of Rb/Sr Ratios in the Loess-paleosol Sequences of Central China During the Last 130,000 Years and Their Implications for Monsoon Paleoclimatology. *Quat. Res.* Vol. 51, pp. 215–219.
- Chen, Z., Cui, J., Ren, Z., Jiang, S., Liang, X., Wang, G., Zou, C., 2019. Geochemistry, Paleoenvironment and Mechanism of Organic-Matter Enrichment in the Lower Silurian Longmaxi Formation Shale in the Sichuan Basin, China. *Acta Geologica Sinica* Vol. 93, No.1, pp. 505-519. <https://doi.org/10.1111/1755-6724.13868>.
- Choi, J.H., and Hariya, Y., 1992. Geochemistry and Depositional Environment of Mn Oxide Deposits in the Tokoro Belt, northeastern Hokkaido, Japan. *Economic Geology*, Vol. 87, No. 5, pp. 1265-1274, <https://doi.org/10.2113/gsecongeo.87.5.1265>.
- Ding, J., Zhang, J., Tang, X., Huo, Z., Han, S., Lang, Y., 2018. Elemental Geochemical Evidence for Depositional Conditions and Organic Matter Enrichment of Black Rock Series Strata in an Inter-Platform Basin: The Lower Carboniferous Datang Formation,

- Southern Guizhou, Southwest China. *Minerals*. Vol.8, No.11, 509, <https://doi:10.3390/min8110509>.
- Dymond, J., Suess, E., Lyle, M., 1992. Barium in Deep-Sea Sediment: a Geochemical Proxy for Paleoproductivity. *Paleoceanography*, Vol. 7, No. 2, pp. 163–181. <https://doi.org/10.1029/92PA00181>.
- Feret, F. R., Roy, D., Boulanger C., 2000. Determination of alpha and beta alumina in ceramic alumina by X-ray diffraction. *Spectrochimica Acta, Part B: Atomic Spectroscopy*, Vol. 55, No. 7, pp. 1051–1061. [https://doi.org/10.1016/S0584-8547\(00\)002252-1](https://doi.org/10.1016/S0584-8547(00)002252-1).
- Fouad, S.F.A., 2015. Tectonic Map of Iraq, SCALE 1: 1000 000, 3rd Edition, 2012. *Iraqi Bulletin of Geology and Mining*, Vol. 11, No. 1, pp. 1-7.
- Guo, L., Jiang, Z., Zhang, J., Li, Y., 2011. Paleoenvironment of Lower Silurian Black Shale and its Significance to the Potential of Shale Gas, Southeast of Chongqing, China. *Energy Explor, Exploit*. Vol. 29, No. 5, pp. 597–616, <https://www.jstor.org/stable/26161188>.
- Helz, G.R., Bura-Nakić, E., Mikac, N., Ciglencečki, I., 2011. New Model for Molybdenum Behavior in Euxinic Waters. *Chemical Geology*, Vol. 284, pp. 323-332. <https://doi.org/10.1016/j.chemgeo.2011.03.012>.
- Herron, M.M., 1988. Geochemical Classification of Terrigenous Sands and Shales from Core or Log Data. *Journal of Sedimentary Research*, Vol. 58, No. 5, pp. 820-829, <https://doi.org/10.1306/212F8E77-2B24-11D7-8648000102C1865D>.
- Hu, J., Li, Q., Song, C., Wang, S., Shen, B., 2017. Geochemical Characteristics of the Permian Sedimentary Rocks from Qiangtang Basin: Constraints for Paleoenvironment and Paleoclimate. *Terr. Atmos. Ocean. Sci.* Vol. 28, pp. 271–282. <https://doi:10.3319/TAO.2016.08.08.01>.
- Hunt, J. M., 1979. *Petroleum Geochemistry and Geology*, Oxford: Freeman, New York, 617 P.
- Jassim, S. Z., and Buday T., 2006 Paleozoic Megasequences (AP1- AP5). In: Jassim SZ, Goff JC (eds) *Geology of Iraq*, Dolin, Prague, and Moravian Museum. Dolin, Prague and Moravian Museum, Czech Republic, pp 91–103.
- Jassim, S.Z., and Goff J. C., 2006. *Geology of Iraq*. Published by Dolin, Prague and Moravian Museum, Berno. 341 P.
- Kettanah, Y.A., Armstrong-Altrin, J.S., Mohammad, F.A., 2021. Petrography and Geochemistry of Siliciclastic Rocks of the Middle Eocene Gercus Formation, Northern Iraq: Implications for Provenance and Tectonic Setting. *Geological Journal*, Vol. 56, No. 5, pp. 2528-2549, <https://doi.org/10.1002/gj.3880>.
- Li, D., Li, R., Zhu, Z., Xu, F., 2018. Elemental Characteristics of Lacustrine Oil Shale and its Controlling Factors of the Palaeo-Sedimentary Environment on Oil Yield: A Case from Chang 7 Oil Layer of Triassic Yanchang Formation in Southern Ordos Basin. *Acta Geochim.* Vol. 37, pp. 228–243. <https://doi.org/10.1007/s11631-017-0206-y>.
- Li, X., Gang, W., Yao, J., Gao, G., Wang, C., Li, J., Liu, Y., Guo, Y., Yang, S., 2020. Major and Trace Elements as Indicators for Organic Matter Enrichment of Marine Carbonate Rocks: A Case Study of Ordovician Subsalt Marine Formations in the Central-Eastern Ordos Basin, North China. *Mar. Pet. Geol.* Vol. 111, pp. 461–475. <https://doi.org/10.1016/j.marpetgeo.2019.08.028>.
- Loucks, R.G., and Ruppel, S.C., 2007. Mississippian Barnett Shale: Lithofacies and Depositional Setting of a Deep-Water Shale-Gas Succession in the Fort Worth Basin, Texas. *AAPG Bulletin* Vol. 91, No. 4, pp. 579–601, <https://doi:10.1306/11020606059>.

- Lyons, D.J., Werne, J.P., Hollander, D.J. Murray, R.W., 2003. Contrasting Sulfur Geochemistry and Fe/Al and Mo/Al Ratios Across the Last Oxidic-to-Anoxic Transition in the Cariaco Basin, Venezuela. *Chemical Geology*. Vol. 195, No. 1-4, pp. 131-157, [https://doi.org/10.1016/S0009-2541\(02\)00392-3](https://doi.org/10.1016/S0009-2541(02)00392-3).
- Marinez, R.F., Kastner, M., Gallego, Y.D., Rodrigo, G.M., Nieto, M.V., Oretga, H.M., 2015. Paleoclimate and Paleoceanography Over the Past 20,000 yr in the Mediterranean Sea Basins as Indicated by Sediment Elemental Proxies, *Quaternary Science Reviews* Vol. 107, pp. 25–46, <https://doi:10.1016/j.quascirev.2014.09.018>.
- McLennan, S.M., 1993. Weathering and global denudation. *J. Geol.* Vol.101, pp.295-303.
- Paytan, A., Kastner, M., Chavez, F.P., 1996. Glacial to interglacial fluctuations in productivity in the equatorial Pacific as indicated by marine barite. *Science*.Vol. 274, pp.1355–1357, <https://doi.org/10.1126/science.274.5291.1355> .
- Scott, C., Slack, J. F., Kelley, K. D., 2017. The hyper-enrichment of V and Zn in black shales of the Late Devonian-Early Mississippian Bakken Formation (USA). *Chemical Geology*. Vol.452, pp.24-33. <https://doi.org/10.1016/j.chemgeo.2017.01.026> .
- Shen, J., Schoepfer, S.D., Feng, Q.L., Zhou, L., Yu, J.X., Song, H.Y., Wei, H.Y., Algeo, T.J., 2015. Marine Productivity Changes During the End-Permian Crisis and Early Triassic Recovery, *Earth Sci. Rev.* Vol. 149, pp. 136–162. <https://doi.org/10.1016/j.earscirev.2014.11.002>.
- Sweere, T., van den Boorn, S., Dickson, A.J., Reichart, G., 2016. Definition of New Trace-Metal Proxies for the Controls on Organic Matter Enrichment in Marine Sediments Based on Mn, Co, Mo, and Cd Concentrations. *Chemical Geology*, Vol. 441, pp. 235–245. <https://doi.org/10.1016/j.chemgeo.2016.08.028>.
- Tao, S., Xu, Y., Tang, D., Xu, H., Li, S., Chen, S., Liu, W., Cui, Y., Gou, M., 2017. Geochemistry of the Shitoumei Oil Shale in the Santanghu Basin, Northwest China: Implications for Paleoclimate Conditions, Weathering, Provenance, and Tectonic Setting, *Int. J. Coal Geol.*, Vol. 184, pp.42–56. <https://doi.org/10.1016/j.coal.2017.11.007>.
- Tenger, W. Liu, Y. Xu, J. Chen, K. Hu, and C. Gao, 2006. Comprehensive Geochemical Identification of Highly Evolved Marine Hydrocarbon Source Rocks: Organic Matter, Paleoenvironment and Development of Effective Hydrocarbon Source Rocks. *Chin. J. Geochem.*, Vol. 25, pp. 333-340, <https://doi:10.1007/s11631-006-0332-4>.
- Tribouillard, N., Algeo, T.J., Lyons, T., Riboulleau, A., 2006. Trace Metals as Paleoredox and Paleoproductivity Proxies: an Update. *Chem. Geol.*, Vol. 232, pp. 12–32. <https://doi.org/10.1016/j.chemgeo.2006.02.012>.
- Tyrrell, T., 1999. The Relative Influences of Nitrogen and Phosphorus on Oceanic Primary Production. *Nature*, Vol. 400, pp. 525–531, <https://doi.org/10.1038/22941>.
- Wang, J. and Guo, S., 2020. Comparison of Geochemical Characteristics of Marine Facies, Marine-Continental Transitional Facies, and Continental Facies Shale in Typical Areas of China and their Control Over Organic-Rich Shale. *Energy Sources, Part A: Recovery, Utilization, and Environmental Effects*, pp. 1-13. <https://doi.org/10.1080/15567036.2020.1796855>.
- Werne, J. P., Sageman, B. B., Lyons, T. W. Hollander, D.J., 2002. An Integrated Assessment of a “Type Euxinic” Deposit: Evidence for Multiple Controls on Black Shale Deposition in the Middle Devonian Oatka Creek Formation. *American Journal of Science*, Vol. 302, No. 2, pp. 110-143, <https://doi.org/10.2475/ajs.302.2.110>.

- Xiao, B., Liu, S. G., Ran, B., Li, Z. W., 2020. Geochemistry and Sedimentology of the Upper Ordovician–Lower Silurian Black Shale in the Northern Margin of the Upper Yangtze Platform, South China: Implications for Depositional Controls on Organic-Matter Accumulation. *Aust. J. Earth Sci.* Vol. 67, No. 1, pp. 129–150, <https://doi.org/10.1080/08120099.2019.1626765>.
- Xu, H., Liu, B., Wu, F., 2010. Spatial and Temporal Variations of Rb/Sr Ratios of the Bulk Surface Sediments in Lake Qinghai. *Geochemistry Transactions*, Vo. 11, No. 3, pp.1-8, <https://doi.org/10.1186/1467-4866-11-3>.
- Zhang, K., Liu, R., Liu, Z., Li, L., Wu, X., Zhao, K., 2020. Influence of Palaeoclimate and Hydrothermal Activity on Organic Matter Accumulation in Lacustrine Black Shales from the Lower Cretaceous Bayingebi Formation of the Yin'e Basin, China. *Palaeogeogr. Palaeoclimatol. Palaeoecol.* Vol. 560, 110007 P., <https://doi.org/10.1016/j.Paleo.2020.110007>.
- Zhang, L., Dong, D., Qiu, Z., Wu, C., Zhang, Q., Wang, Y., Liu, D., Deng, Z., Zhou, S., Pan, S., 2021. Sedimentology and geochemistry of Carboniferous-Permian marine-continental transitional shales in the eastern Ordos Basin, North China. *Palaeogeogr. Palaeoclimatol. Palaeoecol.* Vol. 571, 110389 P., <https://doi.org/10.1016/j.palaeo.2021.110389>.